Deadbeat Predictive Current Control of Permanent-Magnet Synchronous Motors with Stator Current and Disturbance Observer

Xiaoguang Zhang, *Member, IEEE*, Benshuai Hou, and Yang Mei, *Member, IEEE*

***Abstract*—In order to optimize the current-control performance of the permanent-magnet synchronous motor (PMSM) system with model parameter mismatch and one-step control delay, an improved deadbeat predictive current control (DPCC) algorithm for the PMSM drive systems is proposed in this paper. First, the performance of the conventional predictive current control, when parameter mismatch exist, is analyzed, and then a stator current and disturbance observer (SCDO) based on sliding-mode exponential reaching law, which is able to simultaneously predict future value of stator current and track system disturbance caused by parameter mismatch in real time, is proposed. Based on this SCDO, prediction currents are used for replacing the sampled current in DPCC to compensate one-step delay, and estimated parameter disturbances are considered as the feedforward value to compensate the voltage reference calculated by deadbeat predictive current controller. Thus, a composite control method combining the DPCC part and current prediction and feedforward compensation part based on SCDO, called DPCC + SCDO method, is developed. Moreover, based on conventional exponential reaching law, a novel sliding-mode exponential reaching law is proposed to further improve the performance of the DPCC + SCDO method. Simulation and experimental results both show the validity of the proposed current control approach.**

***Index Terms*—Observer, parameter mismatch, permanent-magnet synchronous motor (PMSM), predictive control.**

I. Introduction

DIGITAL control systems of permanent-magnet synchronous machines (PMSMs) are now widely used in industrial applications, due to their high precision, high efficiency, and excellent control performance. In a practical PMSM system, the performance of the current control is the key factor that decides the performance of the system. Therefore, to achieve high steady-state precision and fast dynamic torque response, many current control methods have been studied, and the most common current control methods are hysteresis control [1], proportional–integral (PI) control [2], and predictive control [3]–[9].

Hysteresis control can provide many advantages such as quick current responses, good robustness, and simple algorithm implementation [10], [11]. However, in general, large current ripple and variable switching frequency are difficult to be avoided. The PI-based current control has such advantages as high steady-state control precision and fixed switching frequency, which have been used to improve the static tracking performance of the control system in many applications [12]. However, the PMSM control system is a nonlinear system with unavoidable disturbances, as well as parameter variations. This makes it difficult for PI control algorithms to obtain a satisfying dynamic performance in the entire operating range for this kind of nonlinear systems [13]. Discrete-model-based predictive current control show better steady-state and dynamic performance as compared to hysteresis control and classical PI control [14], [15]. The main objective of this control method is to control motor currents with high accuracy in a transient interval that is as short as possible. Predictive current control basically can be categorized into two groups: model predictive control [16], [17] and deadbeat predictive control [4]–[6], [7]. Model predictive control utilizes system discrete model and inherent discrete nature of motor inverter to forecast the future behavior of states and determines the future voltage vector according to optimization of an operating cost function at each sampling time. The selected voltage vector, which is one of the seven basic vectors and can minimize the cost function, is used for the output of the control system. The advantages of model predictive control, including good capability of handling constraints of system variables, strong robustness, and no pulsewidth modulation (PWM), can ensure an excellent control performance of whole system. However, an inevitable limitations or challenges, i.e., high computational efforts, exist in model predictive control system. In particular, for multistep prediction or for the application of a multilevel converter, the computational efforts rise exponentially [18].

In comparison, the deadbeat predictive control can obtain similar dynamics and better static tracking performances with less computational efforts. This method is based on the motor discrete model to predict voltage references and then translate them into corresponding switching configurations through the

Manuscript received March 18, 2016; revised June 9, 2016; accepted July 12, 2016. Date of publication July 18, 2016; date of current version February 2, 2017. This work was supported in part by the National Natural Science Foundation of China under Grants 51507004 and 51477003, in part by the Natural Science Foundation of Beijing under Grant 4152013, in part by the Scientific Special Foundation of Beijing under Grant PXM2015_014212_000004 and Grant XN053, and in part by the Initial Scientific Research Fund of Young Teachers in North China University of Technology. Recommended for publication by Associate Editor Dr. T. Geyer.

The authors are with the Inverter Technologies Engineering Research Center of Beijing, North China University of Technology, Beijing 100144, China, with the Collaborative Innovation Center of Key Power Energy-Saving Technologies, Beijing 100144, China, and also with the Collaborative Innovation Center of Electric Vehicles, Beijing 100144, China (e-mail: zxg@ncut.edu.cn; junhuige@163.com; meiy@ncut.edu.cn).

Color versions of one or more of the figures in this paper are available online at http://ieeexplore.ieee.org.

Digital Object Identifier 10.1109/TPEL.2016.2592534

space vector PWM (SVPWM) [22]. However, the deadbeat predictive control is absolutely dependent on exact PMSM model, which means that model parameter mismatch would make the calculated voltage references deviate from their expected values. Moreover, control delay of digital control system, including current sampling delay, duty ratio refreshing delay, and other factors, would greatly reduce the system control performance [19]–[22]. In order to solve the aforementioned problems, some methods have been presented [23]–[25]. In [23], a current error-correction technique with the current-regulated delta modulator is presented, which can effectively reduce steady-state error of stator currents. In [24], a robust predictive current control method is designed to reduce the current error between the expected currents and the measured currents, which is caused by inductance parameter mismatch, but the method ignores the effect caused by flux linkage of permanent magnets and resistance mismatch. In [25], predictive control with a parallel integral loop method is presented to compensate for the inaccuracy of the motor model and for the variations of motor parameters. However, it is difficult to tune the integral gain to achieve an acceptable transient response without overshoot.

The combination of predictive control and disturbance observer has been investigated by some researchers to enhance the control performances and compensate the effects of system disturbances [26]–[30]. A nonlinear disturbance observer is utilized to handle disturbances acting of model predictive control on nonlinear systems in [26]. In [27], a disturbance observer is used in the output prediction to correct the errors caused by system disturbances and uncertainties. This approach is validated by its application to a dc–dc buck converter. In [28], the mismatched uncertainties are solved in the sliding-mode control by proposing a novel sliding-mode surface based on the disturbance observer. In order to suppress the disturbances of the nonlinear control system with arbitrary disturbance relative degree, the model predictive control based on generalized nonlinear model and the disturbance observer is proposed in [29]. In [30], in order to counteract the high-order-mismatched disturbances of control system, a novel control method, which is based on incorporating the estimated disturbances and their high-order derivatives, is proposed. And the results show the superior performance of control system in the presence of high-order matched and mismatched disturbances.

The disturbance observers in the aforementioned methods are able to provide precise disturbance compensation. Moreover, with a proper design of observer parameters, it is possible to reduce control sensitivity to model uncertainties, parameter mismatches. However, it is difficult to use these disturbance observers to simultaneously compensate system disturbances and one-step delay in digital control because of lack of state predictive ability.

In this paper, an improved deadbeat predictive current control (DPCC) method is proposed. First, the parameter sensitivity of conventional predictive current control is analyzed, based on the discrete mathematic model of the PMSM. To obtain a better control performance of PMSM digital drive system, when parameter mismatch and one-step delay exist, a stator current and disturbance observer (SCDO), which is able to simultaneously predict future value of stator current and track system disturbance caused by parameter mismatch online, is proposed. The outputs of SCDO, i.e., prediction currents and estimated parameter disturbance, are regarded as compensation parts to compensate one-step delay and voltage reference, respectively. Thus, a composite control approach combining the DPCC part and the current prediction and feedforward compensation part based on SCDO, called the DPCC + SCDO method, is developed. Then, in order to further improve the performance of the DPCC + SCDO method, a novel sliding-mode reaching-law is proposed, which is used to design modified SCDO. Finally, the effectiveness of the proposed current control approach is verified by simulation and experimental results.

II. Machine Mathematical Model

Assuming that the employed PMSM has negligible cross-coupling magnetic saturation, structural asymmetry, iron losses, magnet eddy current loss, and harmonics in the descriptive functions of windings, rotor anisotropy, and coercive force of magnets, the voltage equations of PMSM in synchronous rotating frame can be described as follows [31]:

$$\begin{bmatrix} \frac{di_d}{dt} \\ \frac{di_q}{dt} \end{bmatrix} = \begin{bmatrix} -\frac{R}{L_d} & \omega_e \\ -\omega_e & -\frac{R}{L_q} \end{bmatrix} \cdot \begin{bmatrix} i_d \\ i_q \end{bmatrix} + \begin{bmatrix} \frac{1}{L_d} & 0 \\ 0 & \frac{1}{L_q} \end{bmatrix} \cdot \begin{bmatrix} u_d \\ u_q \end{bmatrix} + \begin{bmatrix} 0 \\ -\frac{\psi_f}{L_q}\omega_e \end{bmatrix}. \quad (1)$$

In this model, u_d and u_q, respectively, represent the *d*- and *q*-axis stator voltages; i_d and i_q are, respectively, the *d*- and *q*-axis currents; L_d=$L_q = L$ is the stator inductance; *R* is the winding resistance; ψ_f is the flux linkage of permanent magnets; and ω_e is the angular velocity (rad/s).

If the sampling period $T_{\rm sc}$ of control system is short enough, the discrete time model of PMSM can be described by the means of a first-order Taylor series expansion. Then the discrete current predictive model of PMSM is shown in (2), where $\boldsymbol{F}$, $\boldsymbol{G}$, and $\boldsymbol{M}$ are given in (3)

$$\begin{bmatrix} i_d(k+1) \\ i_q(k+1) \end{bmatrix} = \boldsymbol{F}(k) \cdot \begin{bmatrix} i_d(k) \\ i_q(k) \end{bmatrix} + \boldsymbol{G} \cdot \begin{bmatrix} u_d(k) \\ u_q(k) \end{bmatrix} + \boldsymbol{M}(k) \quad (2)$$

$$\boldsymbol{F}(k) = \begin{bmatrix} 1 - \frac{T_{\rm sc}R}{L} & T_{\rm sc}\omega_e(k) \\ -T_{\rm sc}\omega_e(k) & 1 - \frac{T_{\rm sc}R}{L} \end{bmatrix}$$

$$\boldsymbol{G} = \begin{bmatrix} \frac{T_{\rm sc}}{L} & 0 \\ 0 & \frac{T_{\rm sc}}{L} \end{bmatrix}$$

$$\boldsymbol{M}(k) = \begin{bmatrix} 0 \\ -\frac{T_{\rm sc}\psi_f}{L}\omega_e(k) \end{bmatrix}. \quad (3)$$

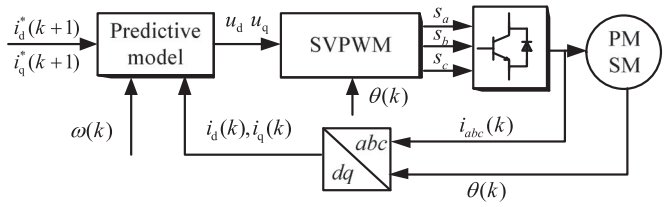

Fig. 1. Block diagram of PMSM DPCC system.

III. Deadbeat Predictive Current Control Method

A. Conventional Deadbeat Predictive Current Control

In conventional DPCC method, according to discrete predictive model (2), the stator voltage of motor that allows the actual current vector to reach the reference currents after a modulation period can be obtained as follows [32]:

$$\begin{bmatrix} u_d(k) \\ u_q(k) \end{bmatrix} = \boldsymbol{G}^{-1} \left\{ \begin{bmatrix} i_d^*(k+1) \\ i_q^*(k+1) \end{bmatrix} - \boldsymbol{F}(k) \cdot \begin{bmatrix} i_d(k) \\ i_q(k) \end{bmatrix} - \boldsymbol{M}(k) \right\} \tag{4}$$

where $i_d^*(k+1)$ and $i_q^*(k+1)$ are the current references.

The structure diagram of PMSM DPCC system is shown in Fig. 1. The voltage vector is computed using the predictive model (4) and then is converted to switching signals through SVPWM modulation.

B. Parameter Sensitivity Analysis

According to (4), it can be found that predictive control models include three parameters (stator resistance, stator inductance, and a permanent magnetic flux linkage), which means that predictive current control is a kind of model-based method. Therefore, the parameter accuracy of predictive models is very important for control performance in a PMSM system. In order to evaluate how the predictive current control is sensitive to a parameter mismatch, parameter sensitivity analysis is focused on in this section.

In a practical control system, the control actions of predictive controller can be described in two steps. In the first step, voltage vectors need to be computed during the sampling period *k* using model (4), in which parameters *R*, *L*, and ψ_f are the crude estimations of the true parameters. These crude estimation values can be determined initially based on the off-line measurement and prior knowledge. In the second step, the computed voltage vector during the sampling period *k* is applied to the real system at the next sampling interval $k+1$ and then the current response of PMSM system can be obtained. This process can be described in (5) and (6), where R_0, L_0 and ψ_{f0} are the true parameters of PMSM

$$\begin{bmatrix} i_d(k+1) \\ i_q(k+1) \end{bmatrix} = \boldsymbol{F}_0(k) \cdot \begin{bmatrix} i_d(k) \\ i_q(k) \end{bmatrix} + \boldsymbol{G}_0 \cdot \begin{bmatrix} u_d(k) \\ u_q(k) \end{bmatrix} + \boldsymbol{M}_0(k) \tag{5}$$

$$\boldsymbol{F}_0(k) = \begin{bmatrix} 1 - \dfrac{T_{\rm sc} R_0}{L_0} & T_{\rm sc}\omega_e(k) \\ -T_{\rm sc}\omega_e(k) & 1 - \dfrac{T_{\rm sc} R_0}{L_0} \end{bmatrix}$$

$$\boldsymbol{G}_0 = \begin{bmatrix} \dfrac{T_{\rm sc}}{L_0} & 0 \\ 0 & \dfrac{T_{\rm sc}}{L_0} \end{bmatrix}$$

$$\boldsymbol{M}_0(k) = \begin{bmatrix} 0 \\ -\dfrac{T_{\rm sc}\psi_{f0}}{L_0}\omega_e(k) \end{bmatrix}. \tag{6}$$

Furthermore, substituting (4) into (5) yields

$$\begin{aligned} i_d(k+1) = {} & \frac{L}{L_0} i_d^*(k+1) + \frac{T_{\rm sc}\Delta R - \Delta L}{L_0} i_d(k) \\ & - \frac{\Delta L}{L_0} T_{\rm sc}\omega_e(k) i_q(k) \end{aligned} \tag{7}$$

$$\begin{aligned} i_q(k+1) = {} & \frac{L}{L_0} i_q^*(k+1) + \frac{T_{\rm sc}\Delta R - \Delta L}{L_0} i_q(k) \\ & - \frac{\Delta L}{L_0} T_{\rm sc}\omega_e(k) i_d(k) + \frac{T_{\rm sc}}{L_0}\Delta\psi_f\omega_e(k) \end{aligned} \tag{8}$$

where $\Delta R = R - R_0$, $\Delta L = L - L_0$, and $\Delta\psi_f = \psi_f - \psi_{f0}$ are the parameter errors between the true system and their crude estimations. Note that i_d (*k* + 1) is approximately equal to i_d(k), and i_q(k+1) is approximately equal to i_q(k) under the steady-state condition. Then (7) and (8) can be simplified as follows:

$$\begin{aligned} i_d(k+1) = {} & \frac{L}{L - T_{\rm sc}\Delta R} i_d^*(k+1) - \frac{\Delta L}{L - T_{\rm sc}\Delta R} \\ & \times T_{\rm sc}\omega_e(k) i_q(k) \end{aligned} \tag{9}$$

$$\begin{aligned} i_q(k+1) = {} & \frac{L}{L - T_{\rm sc}\Delta R} i_q^*(k+1) + \frac{\Delta L}{L - T_{\rm sc}\Delta R} \\ & \times T_{\rm sc}\omega_e(k) i_d(k) + \frac{T_{\rm sc}}{L - T_{\rm sc}\Delta R}\Delta\psi_f\omega_e(k). \end{aligned} \tag{10}$$

Equations (9) and (10) describe the relation between current reference and its response under the condition of model parameter mismatch, which indicates that permanent magnetic flux linkage mismatch only has effect on current i_q; however, stator resistance and inductance both have effect on current i_d and i_q. On the other hand, the one-step delay caused by digital implementation exists in the control system, which can deteriorate the performance of the PMSM system if not considered in the design of the controller [19]–[21]. Therefore, to overcome the influence of model parameter mismatch and one-step delay on control performance, a DPCC method with SCDO is proposed.

IV. Deadbeat Predictive Current Control Method With Stator Current and Disturbance Observer (DPCC + SCDO)

The existence of the parameter mismatch and one-step delay will degrade the control performance if the corresponding

compensation method is not able to suppress it. This paper presents an improved predictive current controller that offers robustness against these two factors. First, a sliding-mode SCDO, which can simultaneously predict future value of stator current and track system disturbance caused by parameter mismatch, is proposed. Using this SCDO, prediction currents are used for replacing the sampled current in DPCC to compensate one-step delay and estimated parameter disturbances are considered as the feedforward value to compensate the voltage reference calculated by deadbeat predictive current controller. Thus, a composite control method combining the DPCC part and current prediction and feedforward compensation part based on SCDO, called DPCC + SCDO method, is developed.

This section is arranged as follows. The SCDO is proposed in Section IV-A, in which the observer stability analysis and the discrete expression of this observer are presented, respectively. Then, the composite control method is proposed in Section IV-B.

A. Proposed Stator Current and Disturbance Observer

According to voltage equation (1), the extended dynamic equation of PMSM can be expressed as follows, when the parameters variations are taken into accounts:

$$\begin{cases} u_d = L\dfrac{di_d}{dt} + Ri_d - \omega_e L i_q + f_d \\ \dfrac{df_d}{dt} = F_d \end{cases} \tag{11}$$

$$\begin{cases} u_q = L\dfrac{di_q}{dt} + Ri_q + \omega_e L i_d + \omega_e \psi_f + f_q \\ \dfrac{df_q}{dt} = F_q \end{cases} \tag{12}$$

where f_d and f_q represent the parameter disturbances, including resistance variation, inductance variation, and permanent magnetic flux linkage variation, and F_d and F_q are the variation rates of parameter disturbances f_d and $f_{q,}$ respectively. Parameter disturbances f_d and f_q can be expressed as follows:

$$\begin{cases} f_d = \Delta L\dfrac{di_d}{dt} + \Delta R i_d - \Delta L \omega_e i_q \\ f_q = \Delta L\dfrac{di_q}{dt} + \Delta R i_q + \Delta L \omega_e i_d + \Delta \psi_f \omega_e \end{cases}. \tag{13}$$

For the purpose of parameter disturbance estimation and current prediction, the SCDO can be designed as follows:

$$\begin{cases} u_d = L\dfrac{d\hat{i}_d}{dt} + R\hat{i}_d - \omega_e L i_q + \hat{f}_d + U_{\text{dsmo}} \\ \dfrac{d\hat{f}_d}{dt} = g_d U_{\text{dsmo}} \end{cases} \tag{14}$$

$$\begin{cases} u_q = L\dfrac{d\hat{i}_q}{dt} + R\hat{i}_q + \omega_e L i_d + \omega_e \psi_f + \hat{f}_q + U_{\text{qsmo}} \\ \dfrac{d\hat{f}_q}{dt} = g_q U_{\text{qsmo}} \end{cases} \tag{15}$$

where $\hat{f}_d$ and $\hat{f}_q$ are the estimates of parameter disturbances f_d and f_q; $\hat{i}_d$ and $\hat{i}_q$ are the estimates of the *d*- and *q*-axis currents; u_d and u_q are the measured voltages, U_{dsmo} and U_{qsmo} represent sliding-mode control function. g_d and g_q are sliding-mode parameter which satisfy equation (16) and will be discussed in next section

$$g_d,\ g_q \in R^+ \tag{16}$$

According to (11), (12), (14), and (15), the error equations can be obtained as

$$\begin{cases} \dfrac{de_1}{dt} = -\dfrac{R}{L}e_1 - \dfrac{1}{L}e_2 - \dfrac{1}{L}U_{\text{dsmo}} \\ \dfrac{de_2}{dt} = g_d U_{\text{dsmo}} - F_d \end{cases} \tag{17}$$

$$\begin{cases} \dfrac{de_3}{dt} = -\dfrac{R}{L}e_3 - \dfrac{1}{L}e_4 - \dfrac{1}{L}U_{\text{qsmo}} \\ \dfrac{de_4}{dt} = g_q U_{\text{qsmo}} - F_q \end{cases} \tag{18}$$

where $e_1 = \hat{i}_d - i_d$ and $e_3 = \hat{i}_q - i_q$ are the current estimation errors and $e_2 = \hat{f}_d - f_d$ and $e_4 = \hat{f}_q - f_q$ are the disturbance estimation errors.

According to sliding-mode control theory, sliding-mode design procedure can be divided into two steps: the first step is sliding-mode surface design, and the second step is to design the sliding-mode control function, which can force the state trajectory converge to the sliding-mode surface. In this paper, the linear sliding-mode surface is chosen, which is expressed as follows:

$$s_d = \hat{i}_d - i_d, \qquad s_q = \hat{i}_q - i_q. \tag{19}$$

However, the design method of conventional sliding-mode control function is only interested in whether the system satisfies the stability criteria but not is concerned about the reaching way the sliding-mode surface, which has important influence on the performance of the sliding-mode system. Therefore, to improve the observation precision of the sliding-mode observer, the exponential reaching law (20) is used to design sliding-mode control function [33]

$$\frac{ds}{dt} = -k_1 \cdot \text{sgn}(s) - \lambda \cdot s \tag{20}$$

where k_1 and λ are the reaching law parameters, both of the values are positive. $\dfrac{ds}{dt} = -\lambda \cdot s$ is index reaching rate whose solution is $s = s(0)e^{-\lambda t}$, $-k_1 \cdot \text{sgn}(s)$ is the sliding-mode control. The reaching time (21) of the exponential reaching law can be calculated by integrating (20) from 0 to t_1, with $s(\text{t}_1) = 0$

$$t_1 = \frac{|s(0)| - \left|\int_0^{t_1} \lambda s dt\right|}{k_1}. \tag{21}$$

One can see from (21) that the reaching speed is increased with high values of k_1 and λ. Therefore, in order to have a faster reaching performance, k_1 and λ should be increased; however, this will directly increase the chattering level because of sliding-mode inherent characteristic. Therefore, in practical application, parameter should be adjusted to find a mean between the convergence speed and the chattering level.

Substituting (19) into (20) yields

$$\begin{cases} \dfrac{de_1}{dt} = -k_1 \cdot \mathrm{sign}(e_1) - \lambda \cdot e_1 \\ \dfrac{de_3}{dt} = -k_1 \cdot \mathrm{sign}(e_3) - \lambda \cdot e_3 \end{cases}. \tag{22}$$

Next, substituting (17) and (18) into (22) yields

$$\begin{cases} -\dfrac{R}{L}e_1 - \dfrac{1}{L}e_2 - \dfrac{1}{L}U_{\mathrm{dsmo}} = -k_1 \cdot \mathrm{sign}(e_1) - \lambda \cdot e_1 \\ -\dfrac{R}{L}e_3 - \dfrac{1}{L}e_4 - \dfrac{1}{L}U_{\mathrm{qsmo}} = -k_1 \cdot \mathrm{sign}(e_3) - \lambda \cdot e_3 \end{cases}. \tag{23}$$

From (23), considering e_2 and e_4 as the disturbances of control function, the sliding-mode control function can be designed as follows:

$$\begin{cases} U_{\mathrm{dsmo}} = (L\lambda - R) \cdot e_1 + k_1 L \cdot \mathrm{sign}(e_1) \\ U_{\mathrm{qsmo}} = (L\lambda - R) \cdot e_3 + k_1 L \cdot \mathrm{sign}(e_3) \end{cases}. \tag{24}$$

1) Observer Stability Analysis: In order to guarantee convergence of the current estimation errors (e_1, e_3) and the disturbance estimation errors (e_2, e_4), observer parameters k_1, g_d, and g_q should be selected reasonably. Therefore, the stability condition of the sliding-mode observer, which is shown in (25), must be satisfied

$$\begin{cases} \dot{V}_d = s_d \cdot \dot{s}_d = e_1 \cdot \dot{e}_1 \le 0 \\ \dot{V}_q = s_q \cdot \dot{s}_q = e_3 \cdot \dot{e}_3 \le 0 \end{cases}. \tag{25}$$

From (17) and (24), the first inequation of stability condition (25) can be rewritten as

$$\begin{aligned} \dot{V}_d &= -\frac{1}{L}e_1(Re_1 + e_2 + U_{\mathrm{dsmo}}) \\ &= -\frac{1}{L}\left[L\lambda e_1^2 + |e_1|\left(k_1 L + \frac{e_2}{\mathrm{sign}(e_1)}\right)\right] \\ &= \begin{cases} -\dfrac{1}{L}[L\lambda e_1^2 + |e_1|(k_1 L + e_2)], & e_1 > 0 \\ -\dfrac{1}{L}[L\lambda e_1^2 + |e_1|(k_1 L - e_2)], & e_1 \le 0 \end{cases}. \end{aligned} \tag{26}$$

To ensure $\dot{V}_d = e_1 \cdot \dot{e}_1 \le 0$, parameter k_1 of the *d*-axis observer should be selected as

$$k_1 > \frac{|e_2|}{L}. \tag{27}$$

Similarly, parameter k_1 of the *q*-axis observer should be selected as

$$k_1 > \frac{|e_4|}{L}. \tag{28}$$

From (27) and (28), it can be found that in order to ensure the whole observer stable, parameter k_1 should be selected as

$$k_1 > \frac{1}{L}\max(|e_2|, |e_4|). \tag{29}$$

Therefore, the proposed sliding-mode observer with parameter k_1 can reach the sliding-mode surface in a finite time and stay on it, which means that errors e_1 and e_3 and their derivatives $\dot{e}_1$ and $\dot{e}_3$ can converge to zero. Then, errors (17) and (18) can be simplified as

$$\begin{cases} \dot{e}_2 + g_d e_2 + F_d = 0 \\ \dot{e}_4 + g_q e_4 + F_q = 0 \end{cases}. \tag{30}$$

The solution for e_2 and e_4 are given as follows:

$$\begin{cases} e_2 = e^{-g_d t}[C + \int F_d \cdot e^{g_d t} dt] \\ e_4 = e^{-g_q t}[C + \int F_q \cdot e^{g_q t} dt] \end{cases} \tag{31}$$

where *C* is a constant. From (31), it can be found that positive value must be selected for parameter g_d and g_q, to ensure the convergence of disturbance error. Moreover, the convergence rates are in direct relation with g_d and g_q.

The aforementioned analysis proves that proposed SCDO is stable with appropriate parameters k_1, g_d, and g_q.

2) Discrete Expression of SCDO: Since the proposed SCDO will be only computed at discrete instants and applied to the system during the sampling interval, the discrete expression of this observer is deduced. For discrete-time system, if the sampling period T_{sc} is short enough, at the time of *k*th sampling period, the discrete expression of current derivation can be given by [34]

$$\frac{di}{dt} = \frac{i(k+1) - i(k)}{T_{\mathrm{sc}}}. \tag{32}$$

Equation (32) is used to discretize (14) and (15), and then the discrete form of SCDO can be expressed as

$$\begin{cases} \hat{i}_d(k+1) = \left(1 - \dfrac{RT_{\mathrm{sc}}}{L}\right)\hat{i}_d(k) + \dfrac{T_{\mathrm{sc}}}{L}u_d(k) \\ \qquad\qquad + T_{\mathrm{sc}}\omega_e(k)i_q(k) - \dfrac{T_{\mathrm{sc}}}{L}\hat{f}_d(k) - \dfrac{T_{\mathrm{sc}}}{L}U_{\mathrm{dsmo}}(k) \\ \hat{f}_d(k+1) = \hat{f}_d(k) + T_{\mathrm{sc}} g_d U_{\mathrm{dsmo}}(k) \end{cases} \tag{33}$$

$$\begin{cases} \hat{i}_q(k+1) = \left(1 - \dfrac{RT_{\mathrm{sc}}}{L}\right)\hat{i}_q(k) + \dfrac{T_{\mathrm{sc}}}{L}u_q(k) - T_{\mathrm{sc}}\omega_e(k)i_d(k) \\ \qquad\qquad - \dfrac{T_{\mathrm{sc}}\psi_f}{L}\omega_e(k) - \dfrac{T_{\mathrm{sc}}}{L}\hat{f}_q(k) - \dfrac{T_{\mathrm{sc}}}{L}U_{\mathrm{qsmo}}(k) \\ \hat{f}_q(k+1) = \hat{f}_q(k) + T_{\mathrm{sc}} g_q U_{\mathrm{qsmo}}(k) \end{cases} \tag{34}$$

where $\hat{i}_d(k+1)$ and $\hat{i}_q(k+1)$ represent the predictive future values of stator currents and $\hat{f}_d(k+1)$ and $\hat{f}_q(k+1)$ are the predictive values of the estimated parameter disturbances. $U_{\mathrm{dsmo}}(k)$ and $U_{\mathrm{qsmo}}(k)$ satisfy $U_{\mathrm{dsmo}}(k) = (L\lambda - R) \cdot e_1(k) + k_1 L \cdot \mathrm{sign}(e_1(k))$ and $U_{\mathrm{qsmo}}(k) = (L\lambda - R) \cdot e_3(k) + k_1 L \cdot \mathrm{sign}(e_3(k))$, in which $e_1(k) = \hat{i}_d(k) - i_d(k)$ and $e_3 = \hat{i}_q(k) - i_q(k)$. The discrete block diagram of SCDO is illustrated in Fig. 2.

B. DPCC + SCDO Method

By replacing the sampled current in (4) with the predicted current value of SCDO and compensating parameter disturbances with the estimated disturbance value of SCDO, the proposed DPCC + SCDO method, which includes DPCC part, current prediction and disturbance feedforward compensation, can be

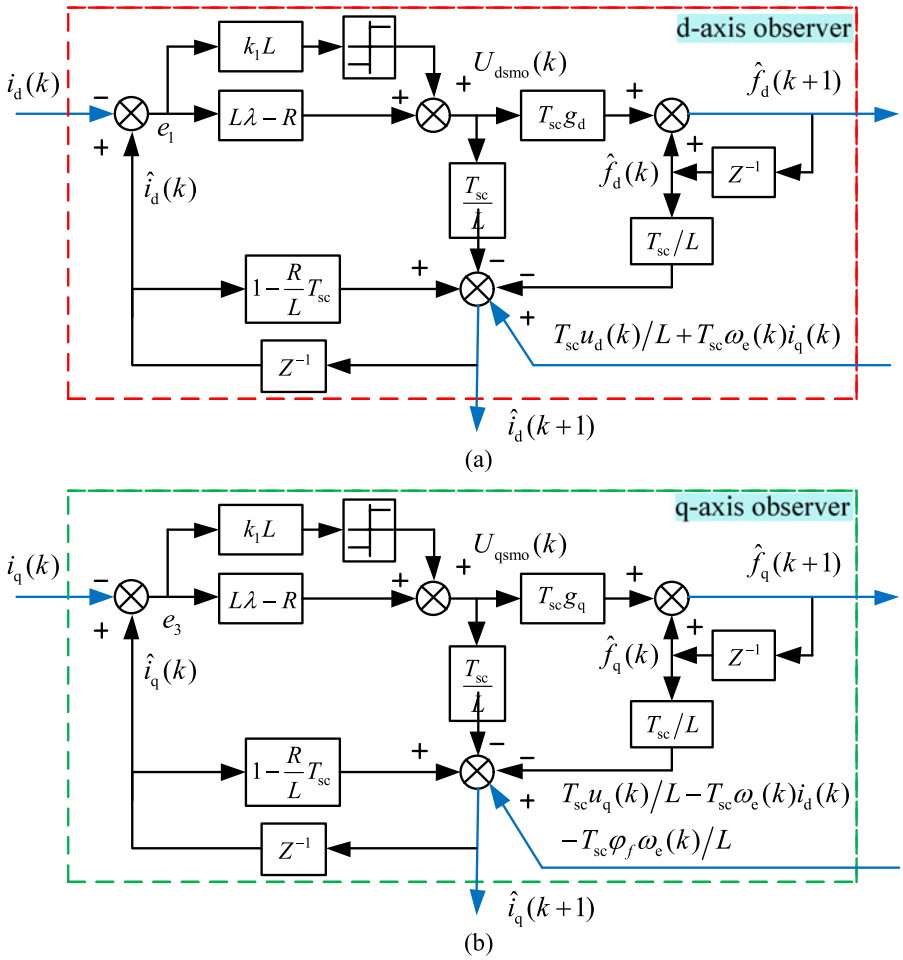

Fig. 2. Discrete block diagram of proposed SCDO: (a) *d*-axis observer and (b) *q*-axis observer.

expressed as follows:

$$\begin{aligned} U_d^* &= u_d(k) + \hat{f}_d(k+1) \\ U_q^* &= u_q(k) + \hat{f}_q(k+1) \end{aligned} \tag{35}$$

where U^{*d} and U^{*q} represent the voltage output of controller and $u_d(k)$ and $u_q(k)$ are given by

$$\begin{bmatrix} u_d(k) \\ u_q(k) \end{bmatrix} = \boldsymbol{G}^{-1} \left\{ \begin{bmatrix} i_d^*(k+1) \\ i_q^*(k+1) \end{bmatrix} - \boldsymbol{F}(k) \cdot \begin{bmatrix} \hat{i}_d(k+1) \\ \hat{i}_q(k+1) \end{bmatrix} - \boldsymbol{M}(k) \right\}. \tag{36}$$

The block diagram of the DPCC + SCDO method is shown in Fig. 3, and the flowchart of DPCC + SCDO method is shown in Fig. 4. In novel controller (35), variables $u_d(\mathrm{k})$ and $u_q(\mathrm{k})$ can be obtained by predicted current values of SCDO, which can compensate one-step delay in conventional DPCC (4). Moreover, the parameter disturbances can be estimated and compensated online, which will improve the regulation ability of predictive current control system.

V. Deadbeat Predictive Current Control Method With Adaptive Stator Current and Disturbance Observer (DPCC + ASCDO)

This section is arranged as follows. The adaptive sliding-mode reaching law based on conventional sliding-mode exponential reaching law is proposed in Section V-A. Then a comparative analysis between the conventional exponential reaching law and the adaptive sliding-mode reaching law is presented in Section V-B. Finally, the novel composite control method is designed in Section V-C.

A. Proposed Adaptive Sliding-Mode Reaching Law

To further improve the control performance of DPCC + SCDO method, an adaptive SCDO based on a novel adaptive sliding-mode reaching law (called ASCDO) is presented in this section. Based on conventional sliding-mode exponential reaching law, an adaptive sliding-mode reaching law is proposed, which is realized based on the choice of an exponential term that adapts to the sliding-mode variations. The novel reaching law is expressed as follows:

$$\frac{ds}{dt} = -M \cdot \mathrm{sgn}(s) - \lambda s, \qquad M = \frac{k}{\varepsilon + \left(1 + \dfrac{1}{|x|} - \varepsilon\right) e^{-\delta|s|}} \tag{37}$$

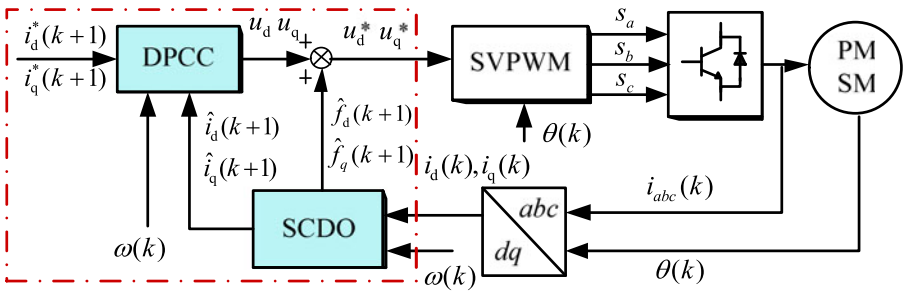

Fig. 3. Block diagram of DPCC + SCDO method.

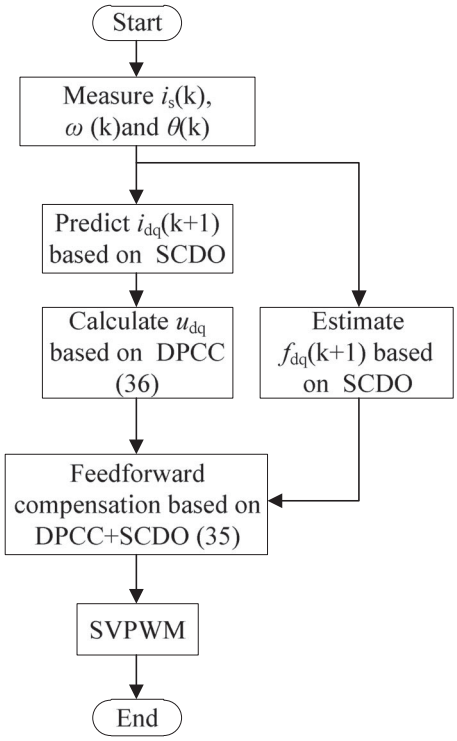

Fig. 4. Flowchart of DPCC + SCDO method.

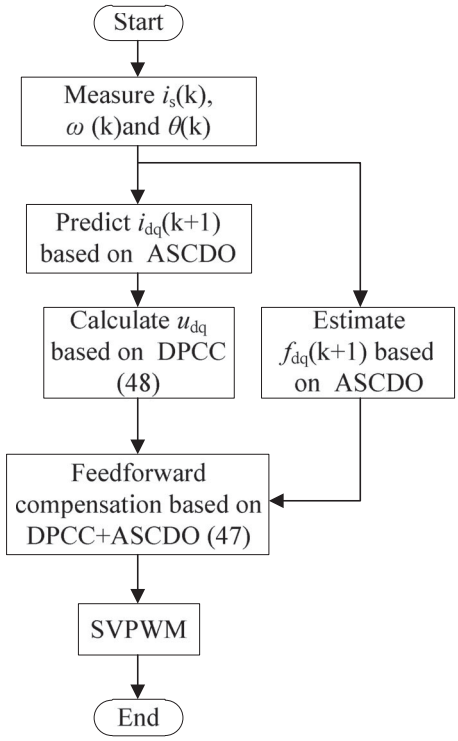

Fig. 5. Flowchart of DPCC + ASCDO method.

where $k > 0$, $\delta > 0$, and $0 < \varepsilon < 1$. x is the system state, and s represent the sliding-mode surface. And parameters k and λ in (37) have the same meaning with k_1 and λ in (20).

In (37), it can be observed that if sliding mode $|s|$ increases, variable M converges to k/ε that is greater than the value of k in the exponential reaching law. This means that compared with the exponential reaching law, the novel reaching law has a faster reaching speed. On the other hand, if sliding mode $|s|$ decreases, variable M converges to $k|x|/(1+|x|)$, in which state $|x|$ gradually decreases to 0 with the sliding-mode control function. This means that when the system trajectory approaches the sliding-mode surface $s = 0$, variable M gradually decreases to 0 to suppress sliding-mode chattering. Thus, SCDO using this adaptive reaching law can dynamically adapt to the variations of the sliding-mode surface by making variable M vary between 0 and value of k/ε.

TABLE I
PARAMETERS OF THE PMSM CONTROL SYSTEM

d- and q-axis inductances	$L_d = L_q = 9$ mH
Stator phase resistance	$R = 2.6\ \Omega$
Viscous friction coefficient	$B = 0.003$ N·m·s/rad
Number of pole pairs	$P = 4$
Rotational inertia	$J = 0.0102$ kg·m^2
Flux linkage of permanent magnets	$\psi_a = 0.175$Wb

B. Comparative Analysis Between the Exponential Reaching Law and the Novel Reaching Law

The reaching time and chattering level of two kinds of reaching law are discussed in this section. First, from the novel reaching law (37), the reaching time t, i.e., the required time for system states to reach sliding-mode surface $s = 0$, can be

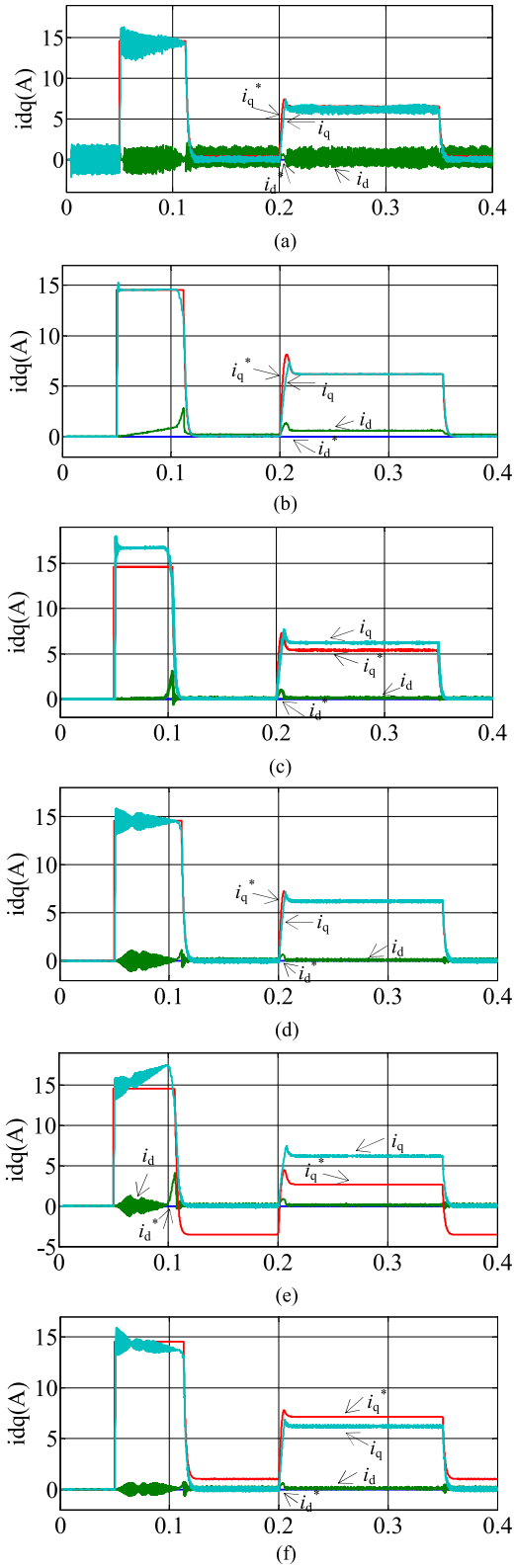

Fig. 6. Simulation results of conventional DPCC under parameters mismatch. (a) L= 2L_0. (b) L= 0.5L_0. (c) R= 10R_0. (d) R= 0.1R_0. (e) ψ_f = 4 ψ_{f0}. (f) ψ_f = 0.25 ψ_{f0}.

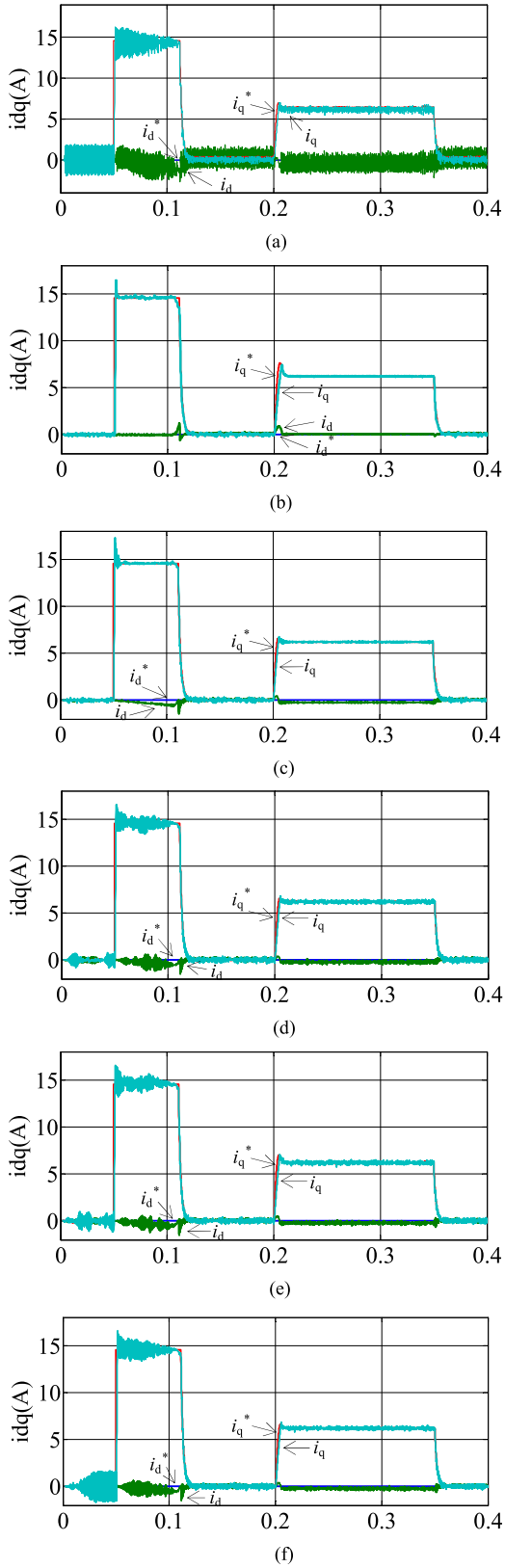

Fig. 7. Simulation results of DPCC + SCDO under parameters mismatch. (a) L= 2L_0. (b) L= 0.5L_0. (c) R= 10R_0. (d) R= 0.1R_0. (e) ψ_f = 4 ψ_{f0}. (f) ψ_f = 0.25ψ_{f0}.

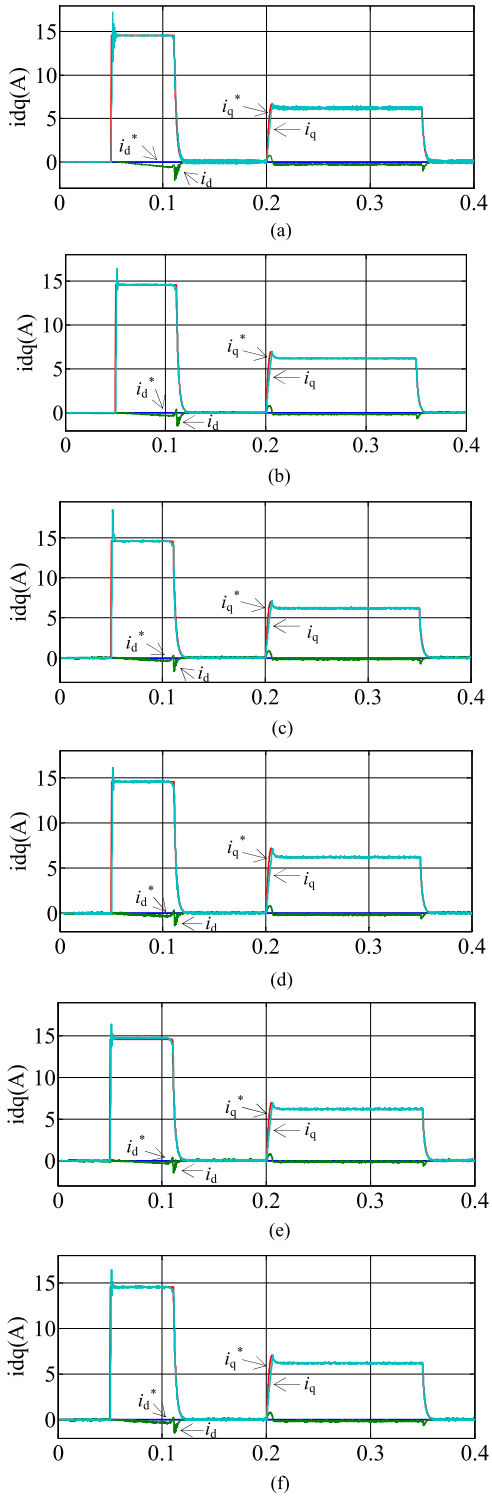

Fig. 8. Simulation results of DPCC + ASCDO under parameters mismatch. (a) L= 2L$_0$. (b) L= 0.5L$_0$. (c) R= 10R$_0$. (d) R= 0.1R$_0$. (e) $\psi_f = 4\ \psi_{f0}$. (f) $\psi_f = 0.25\ \psi_{f0}$.

computed as

$$\left(\frac{ds}{dt}+\lambda s\right)\left[\varepsilon+\left(1+\frac{1}{|x|}-\varepsilon\right)e^{-\delta|s|}\right]=-k\ \mathrm{sgn}(s). \quad (38)$$

With $s(t) = 0$, integrating (38) from 0 to t yields

$$t=\frac{\left(1+\frac{1}{|x|}-\varepsilon\right)[|A|+\lambda C]-\varepsilon s(0)+\lambda\varepsilon B}{-k} \quad (39)$$

where $A=\int_0^t e^{-\delta|s|}ds$, $B=\int_0^t sdt$, and $C=\int_0^t se^{-\delta|s|}dt$.

Since $1-\mathrm{e}^{-\delta|\mathrm{s}(0)|}<1$ and parameter δ can be chosen such that $\delta >> (1+\frac{1}{|x|}-\varepsilon)$, the equality (39) can be simplified as

$$t<\frac{\varepsilon\,|s(0)|+\lambda\varepsilon\,|B|}{k}. \quad (40)$$

It can be found from (40) that parameter δ has no influence on reaching time of novel reaching law, and the smaller the value of ε is, the shorter the reaching time will be. Therefore, in order to have a faster tracking performance of observer, a smaller value of ε should be chosen.

Then substituting $t = t_1+\Delta t$ and $B=\int_0^t sdt$ into inequality (40) yields

$$t<\frac{\varepsilon\,|s(0)|-\varepsilon\left|\int_0^{t_1}\lambda sdt+\int_{t_1}^{t_1+\Delta t}\lambda sdt\right|}{k} \quad (41)$$

where t_1 is the reaching time of the exponential reaching law and Δt is the time difference between the exponential reaching law and the novel reaching law. Noticing that inequality $|\int_0^{t_1}\lambda sdt+\int_{t_1}^{t_1+\Delta t}\lambda sdt|\le|\int_0^{t_1}\lambda sdt|+|\int_{t_1}^{t_1+\Delta t}\lambda sdt|$ is always correct, the following inequality can be obtained:

$$t<\frac{\varepsilon\,|s(0)|-\varepsilon\left(\left|\int_0^{t_1}\lambda sdt\right|+\left|\int_{t_1}^{t_1+\Delta t}\lambda sdt\right|\right)}{k}. \quad (42)$$

Thus, from (21) and (42), the time difference between the reaching time t of the novel reaching law and t_1 of the exponential reaching law with the same gain $k=\mathrm{k}_1$ can be obtained as follows:

$$\begin{aligned}t_1-t>&\ \frac{|s(0)|-\left|\int_0^{t_1}\lambda sdt\right|}{k_1}\\&-\frac{\varepsilon\,|s(0)|-\varepsilon\left|\int_0^{t_1}\lambda sdt\right|-\varepsilon\left|\int_{t_1}^{t_1+\Delta t}\lambda sdt\right|}{k}\\=&\ \frac{|s(0)|-\left|\int_0^{t_1}\lambda sdt\right|}{k}(1-\varepsilon)+\frac{\varepsilon\left|\int_{t_1}^{t_1+\Delta t}\lambda sdt\right|}{k}.\end{aligned} \quad (43)$$

Note that the value of $1-\varepsilon$ is always positive; then (43) implies that $t_1-\mathrm{t}>0$, which means that the proposed reaching law has faster reaching time compared with the exponential reaching law.

On the other hand, to evaluate the chattering level of two different reaching laws, the same reaching time, i.e., t=t$_1$ and $\Delta t = 0$, is chosen; then the following expression can be obtained:

$$k=\varepsilon k_1. \quad (44)$$

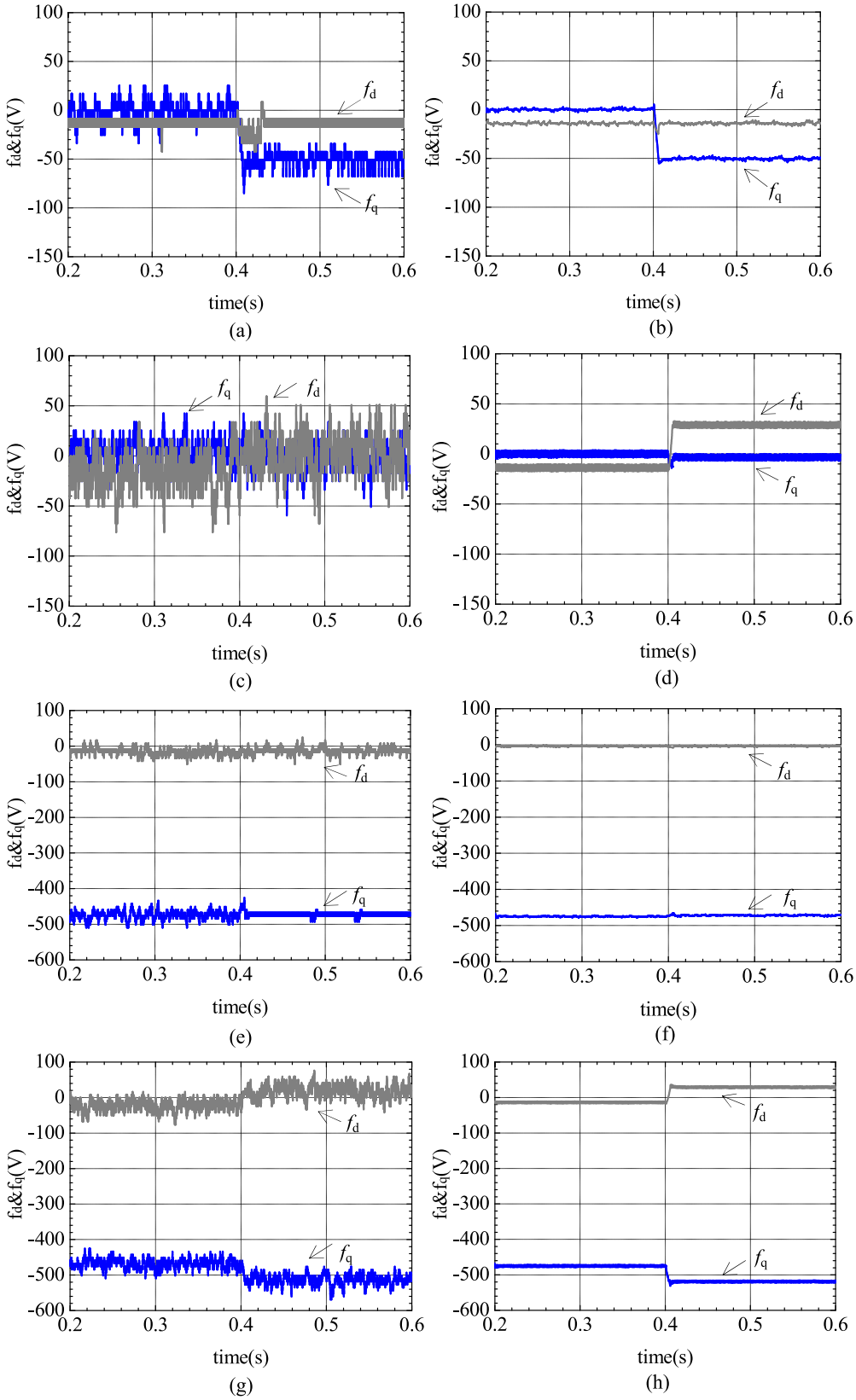

Fig. 9. Disturbance estimation results of SCDO and ASCDO under parameter mismatch $R{=}\ 10\mathrm{R}_0$, $L{=}\ 2\mathrm{L}_0$ and $\psi_f = 4\ \psi_{f0}$. (a) Observation value of SCDO under $R{=}\ 10\mathrm{R}_0$. (b) Observation value of ASCDO under $R{=}\ 10\mathrm{R}_0$. (c) Observation value of SCDO under $L{=}\ 2\mathrm{L}_0$. (d) Observation value of ASCDO under $L{=}\ 2\mathrm{L}_0$. (e) Observation value of SCDO under $\psi_f = 4\ \psi_{f0}$. (f) Observation value of ASCDO under $\psi_f = 4\ \psi_{f0}$. (g) Observation value of SCDO under $R{=}\ 10\mathrm{R}_0$, $L{=}\ 2\mathrm{L}_0$, and $\psi_f = 4\ \psi_{f0}$. (h) Observation value of ASCDO under $R{=}\ 10\mathrm{R}_0$, $L{=}\ 2\mathrm{L}_0$, and $\psi_f = 4\ \psi_{f0}$.

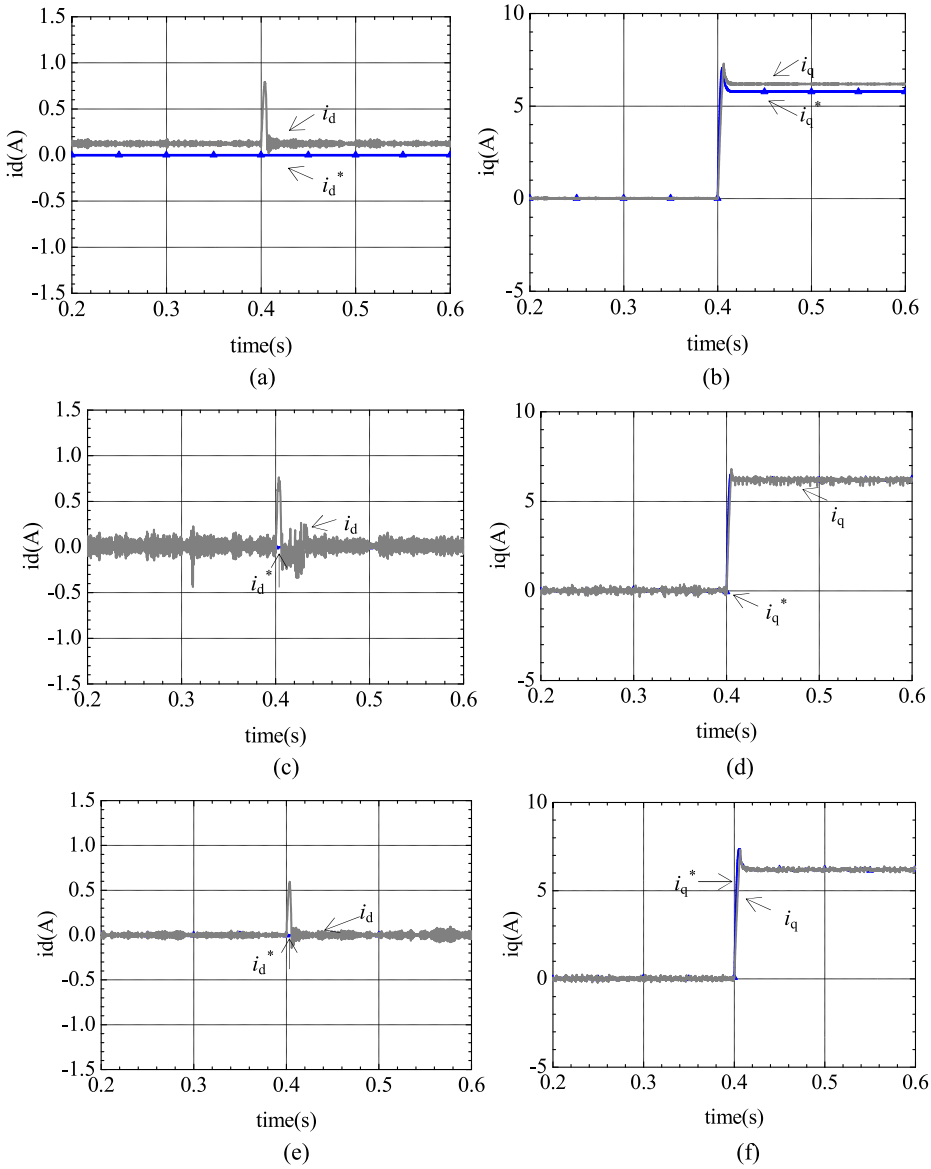

Fig. 10. Experimental results of three current control methods under $R = 10\mathrm{R}_0$. (a) d-Axis current reference and its response with DPCC method. (b) q-Axis current reference and its response with DPCC method. (c) d-Axis current reference and its response with DPCC + SCDO method. (d) q-Axis current reference and its response with DPCC + SCDO method. (e) d-Axis current reference and its response with DPCC + ASCDO method. (f) q-Axis current reference and its response with DPCC + ASCDO method.

Therefore, it proves that gain k is less than k_1, which indicates that the proposed adaptive reaching law has smaller sliding-mode chattering under the condition of same reaching time.

C. DPCC + ASCDO Method

To further improve the control performance of predictive current control system, ASCDO is used to replace SCDO in this session.

Similarly, according error (17) and (18) and novel reaching law (37), the following equation can be obtained:

$$\begin{cases} -\dfrac{R}{L}e_1 - \dfrac{1}{L}e_2 - \dfrac{1}{L}U_{\mathrm{dsmo}} = -M\cdot\mathrm{sign}(e_1) - \lambda\cdot e_1 \\ -\dfrac{R}{L}e_3 - \dfrac{1}{L}e_4 - \dfrac{1}{L}U_{\mathrm{qsmo}} = -M\cdot\mathrm{sign}(e_3) - \lambda\cdot e_3 \end{cases}. \quad (45)$$

Then the sliding-mode control function of ASCDO using the novel reaching law can be designed as follows:

$$\begin{cases} U_{\mathrm{dsmo}} = (L\lambda - R)\cdot e_1 + ML\cdot\mathrm{sign}(e_1) \\ U_{\mathrm{qsmo}} = (L\lambda - R)\cdot e_3 + ML\cdot\mathrm{sign}(e_3) \end{cases}. \quad (46)$$

If parameters of ASCDO are also selected based on (29) and (31), this observer is stable. Then, similar to (35), we can design DPCC + ASCDO approach as follows:

$$\begin{aligned} U_d^* &= u_d^m(k) + \hat{f}_d^m(k+1) \\ U_q^* &= u_q^m(k) + \hat{f}_q^m(k+1) \end{aligned} \quad (47)$$

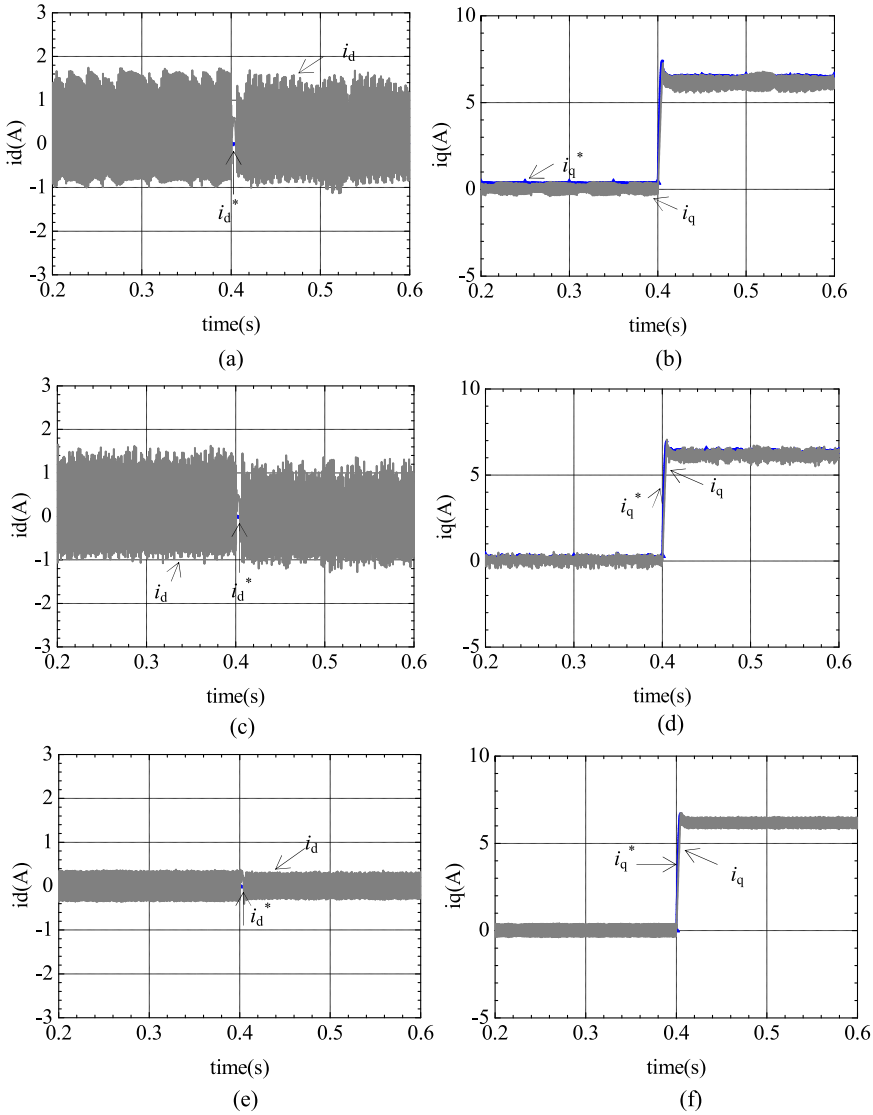

Fig. 11. Experimental results of three current control methods under $L = 2L_0$. (a) d-Axis current reference and its response with DPCC method. (b) q-Axis current reference and its response with DPCC method. (c) d-Axis current reference and its response with DPCC + SCDO method. (d) q-Axis current reference and its response with DPCC + SCDO method. (e) d-Axis current reference and its response with DPCC + ASCDO method. (f) q-Axis current reference and its response with DPCC + ASCDO method.

where $\hat{f}_d^m(k+1)$ and $\hat{f}_q^m(k+1)$ are the disturbance estimates of ASCDO. $u_d^m(k)$ and $u_q^m(k)$ are given by

$$\begin{bmatrix} u_d^m(k) \\ u_q^m(k) \end{bmatrix} = \boldsymbol{G}^{-1} \left\{ \begin{bmatrix} i_d^*(k+1) \\ i_q^*(k+1) \end{bmatrix} - \boldsymbol{F}(k) \cdot \begin{bmatrix} \hat{i}_d^m(k+1) \\ \hat{i}_q^m(k+1) \end{bmatrix} - \boldsymbol{M}(k) \right\} \quad (48)$$

where $\hat{i}_d^m(k+1)$ and $\hat{i}_q^m(k+1)$ are the predicted current values of ASCDO. The flowchart of DPCC + ASCDO method is shown in Fig. 5.

VI. Simulation and Experimental Results

In this section, to demonstrate the effectiveness of the proposed predictive current control approach, simulations and experiments of the conventional DPCC method, the DPCC + SCDO method, and the DPCC + ASCDO method in one PMSM system were carried out. Simulations are established in MATLAB/Simulink. The experiments platform is constructed by TI processor and the sampling frequency is 10 kHz. In addition, the parameters of PMSM are listed in Table I. The simulation parameters are $k_1 = 220$, $\lambda = 50$, $\delta = 2$, $\varepsilon = 0.1$, and $g_d = g_q = 850$.

The simulation results of current references and current responses with different parameter mismatch are shown in Figs. 6, 7, and 8. In the figures, the red line is reference of the q-axis current, and the blue line is reference of the d-axis current. At 0.05 s, the speed reference steps from 0 to 1400 r/min. And at 0.2 and 0.35 s, the load torque is increased suddenly from 0 to 10 N · m and decreased from 10 to 0 N·m, respectively. In Fig. 6, the conventional DPCC simulation results are shown under the condition of model parameter mismatch. According to the simulation results, it can be observed that parameter mismatch,

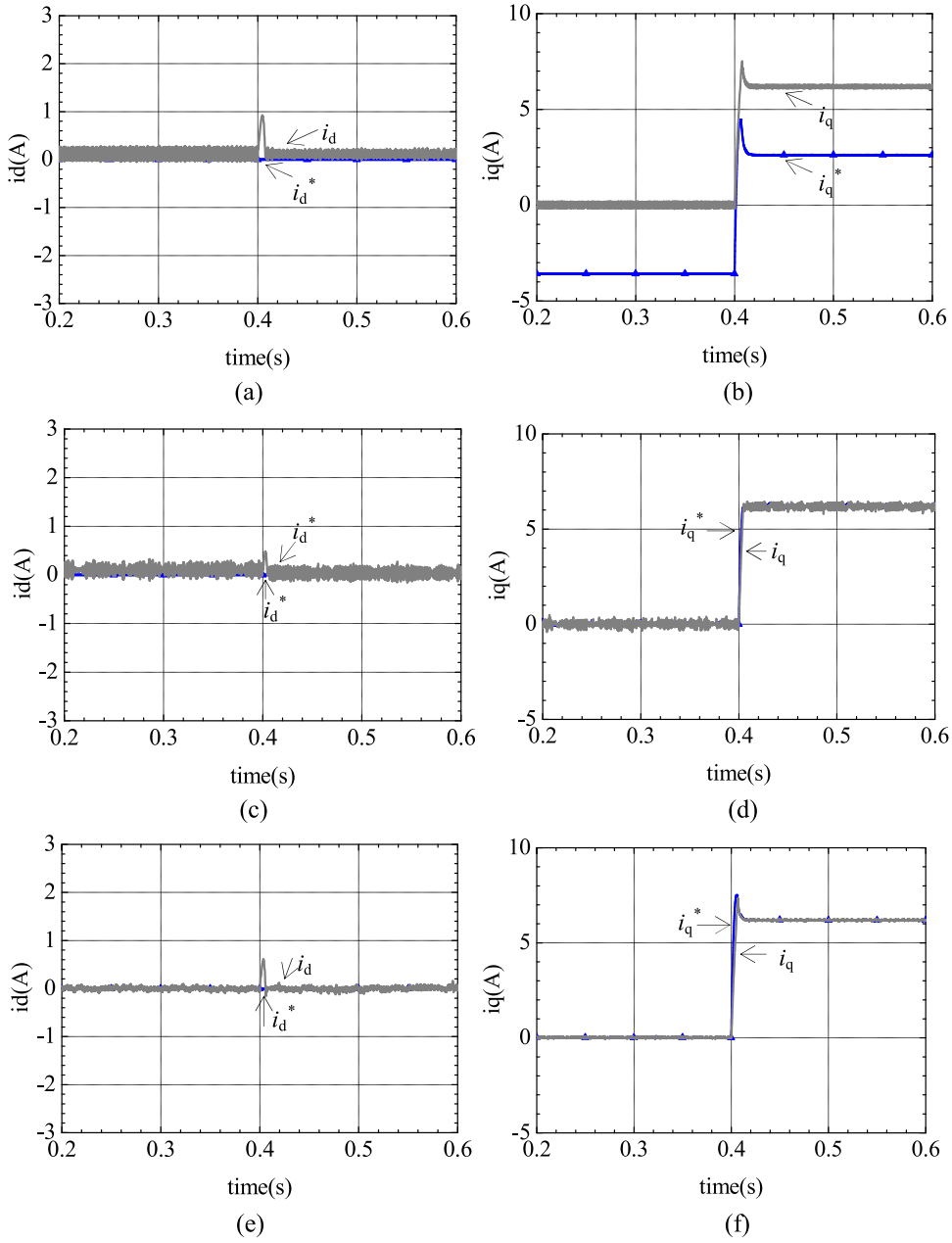

Fig. 12. Experimental results of three current control methods under $\psi_f = 4\ \psi_{f0}$. (a) d-Axis current reference and its response with DPCC method. (b) q-Axis current reference and its response with DPCC method. (c) d-Axis current reference and its response with DPCC + SCDO method. (d) q-Axis current reference and its response with DPCC + SCDO method. (e) d-Axis current reference and its response with DPCC + ASCDO method. (f) q-Axis current reference and its response with DPCC + ASCDO method.

including inductance, resistance, and flux linkage of permanent magnets mismatch, has effect on current responses in conventional DPCC method. Moreover, Figs. 7 and 8 show the simulation results of the DPCC + SCDO method and the DPCC + ASCDO method, respectively. It is obvious that both DPCC + SCDO method and DPCC + ASCDO method can track current references exactly and quickly; however, DPCC + ASCDO method has better steady-state performance due to the application of the novel sliding-mode reaching law.

The experimental results of three current control methods (DPCC, DPCC + SCDO, and DPCC + ASCDO) are shown in Figs. 9−13, when the load torque (10 N·m) is added suddenly. In the practical experiment, proposed DPCC + SCDO method and DPCC + ASCDO method need to be used to compute voltage vectors by (35) and (36) and (47) and (48), respectively, in which parameters R, L, and ψ_f are the crude estimations of the true parameters. These crude estimation values can be utilized to simulate parameter mismatch based on true parameters of PMSM (R_0, L_0, and ψ_{f0}). The experimental parameters are $k_1 = 245$, $\lambda = 40$, $\delta = 2$, $\varepsilon = 0.1$, and $g_d = g_q = 880$.

In order to evaluate the performance of the proposed sliding-mode reaching law, the experiments of SCDO using conventional exponential reaching law and ASCDO using the proposed reaching law have been completed. The results are shown

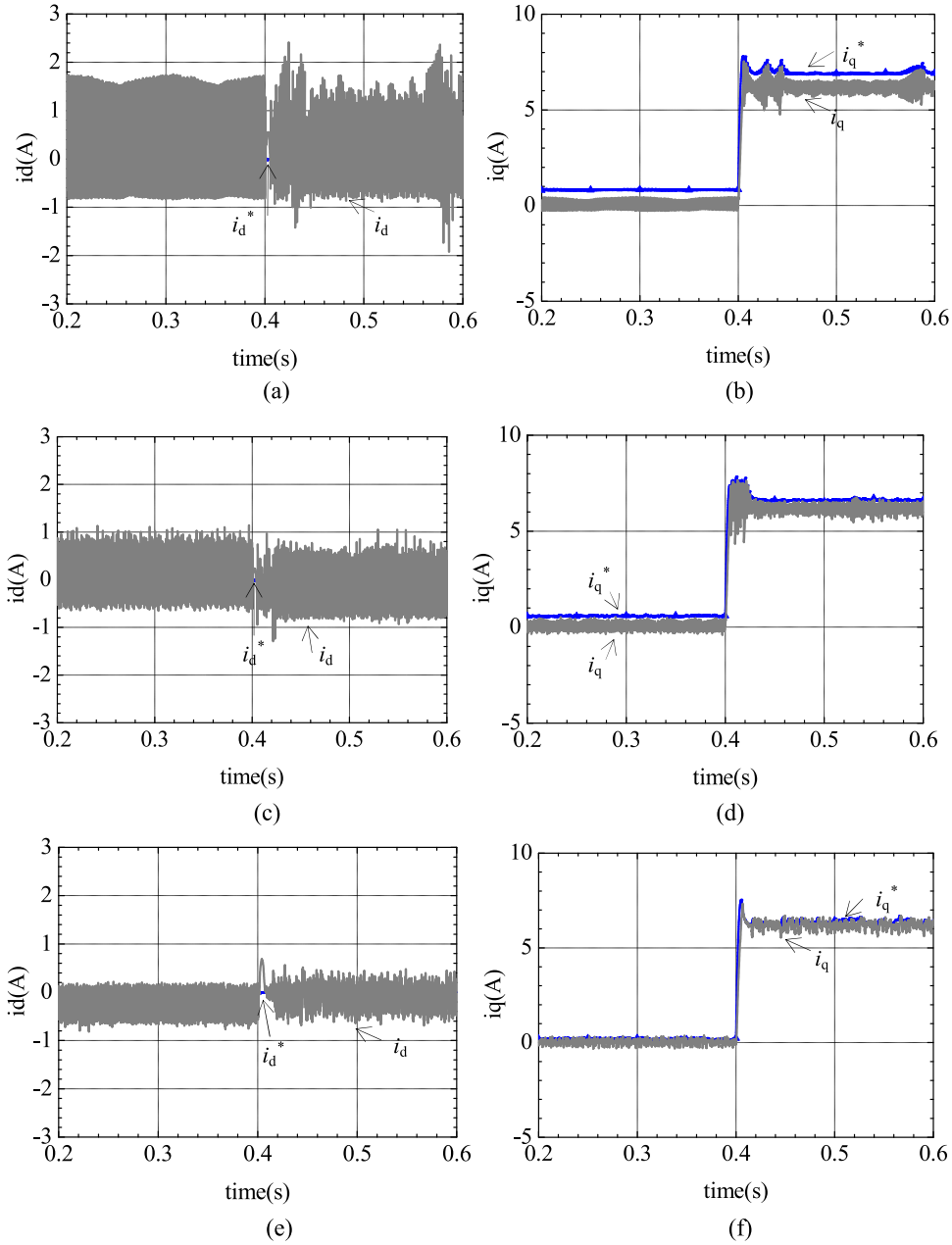

Fig. 13. Experimental results of three current control methods under $R{=}\ 0.1\mathrm{R}_0$, $L{=}\ 0.5\mathrm{L}_0$ and $\psi_f\ =0.25\ \psi_{f0}$. (a) d-Axis current reference and its response with DPCC method. (b) q-Axis current reference and its response with DPCC method. (c) d-Axis current reference and its response with DPCC + SCDO method. (d) q-Axis current reference and its response with DPCC + SCDO method. (e) d-Axis current reference and its response with DPCC + ASCDO method. (f) q-Axis current reference and its response with DPCC + ASCDO method.

in Fig. 9, and the ripple quantitative comparison under different parameter mismatch is shown in Table II can be obtained from the response, when the load torque is changed from 0 to 10 N·m. It is seen that the ripples of disturbance estimate of ASCDO are much reduced compared to SCDO. At the state of $R{=}\ 10R_0$, the f_d ripple of ASCDO is reduced by up to 68%, from 6.18 to 1.98 V. The f_q ripple of ASCDO is reduced by up to 89%, from 23.01 to 2.56 V. At the state of $L{=}\ 2L_0$, the f_d ripple of ASCDO is reduced by up to 90%, from 51.78 to 5.09 V. The f_q ripple of ASCDO is reduced by up to 86%, from 35.02 to 4.56 V. At the state of $\psi_f\ =0.25\ \psi_{f0}$, the f_d ripple of ASCDO is reduced by up to 88%, from 22.12 to 2.54 V. The f_q ripple of ASCDO is reduced by up to 87%, from 24.88 to 3.35 V. At the state of $R{=}\ 10\mathrm{R}_0$, $L{=}\ 2\mathrm{L}_0$, and $\psi_f\ =0.25\ \psi_{f0}$, the f_d ripple of ASCDO is reduced by up to 88%, from 43.91 to 5.09 V. The f_q ripple of ASCDO is reduced by up to 85%, from 40.87 to 5.86 V. Experimental results indicate that the proposed reaching law can reduce the sliding-mode chattering level of observer and the ASCDO using novel reaching law has better observer performance compared with SCDO using conventional reaching law.

Figs. 10−12 shows the current response comparisons of three different control methods under $R{=}\ 10\mathrm{R}_0$, $L{=}\ 2\mathrm{L}_0$, and $\psi_f\ =4\ \psi_{f0}$, respectively. Similarly, Fig. 13 displays the current

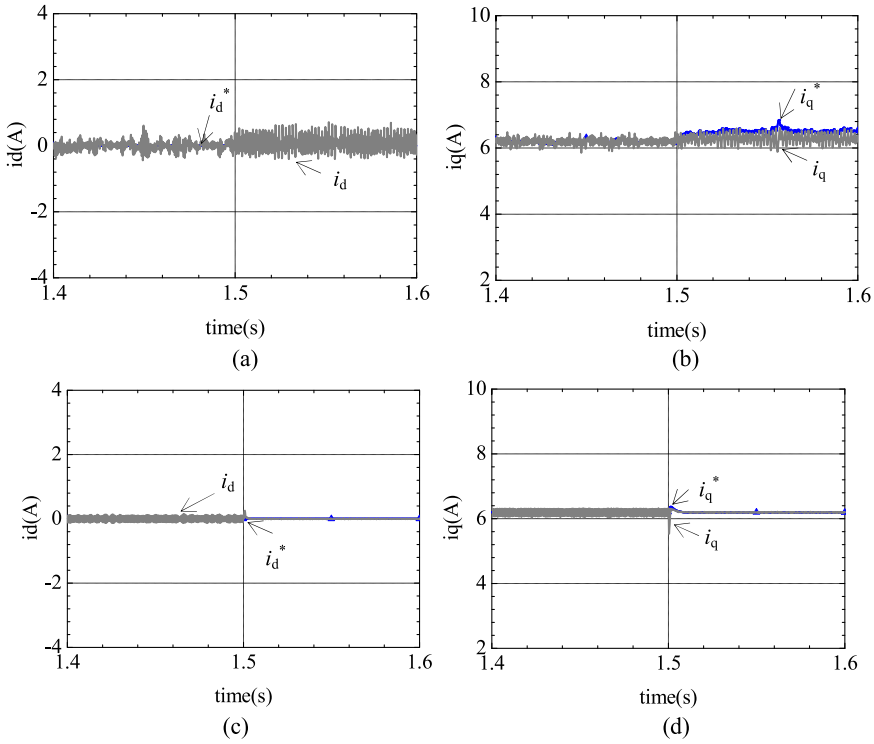

Fig. 14. Experimental results of proposed methods when a step change of parameter occurs at 1.5 s (from R_0, L_0, and ψ_{f0} change to $1.5\mathrm{R}_0$, $0.5\mathrm{L}_0$, and $0.5\,\psi_{f0}$). (a) *d*-Axis current reference and its response with DPCC + SCDO method. (b) *q*-Axis current reference and its response with DPCC + SCDO method. (c) *d*-Axis current reference and its response with DPCC + ASCDO method. (d) *q*-Axis current reference and its response with DPCC + ASCDO method.

TABLE II
TIPPLE QUANTITATIVE COMPARISON OF SCDO AND ASCDO UNDER DIFFERENT PARAMETER MISMATCH

Parameter mismatch	Methods	f_{d} ripple (V)	f_{q} ripple (V)
$R{=}10R_0$ $L{=}2L_0$ $\Psi_f{=}4\,\Psi_{f0}$	SCDO	43.91	40.87
	ASCDO	5.09	5.86
$R = 10R_0$	SCDO	6.18	23.01
	ASCDO	1.98	2.56
$L = 2L_0$	SCDO	51.78	35.02
	ASCDO	5.09	4.56
$\Psi = 4\Psi_{f0}$	SCDO	22.12	24.88
	ASCDO	2.54	2.35

TABLE III
QUANTITATIVE COMPARISON OF DPCC, DPCC+SCDO AND DPCC+ASCDO UNDER DIFFERENT PARAMETER MISMATCH

Parameter mismatch	Methods	i_{d} ripple (A)	i_{q} ripple (A)	i_{d} error (A)	i_{q} error (A)
$R{=}0.1R_0$ $L{=}0.5L_0$ $\Psi_f{=}0.25\,\Psi_{f0}$	DPCC	2.2	1.5	0.52	0.8
	DPCC+SCDO	0.95	0.54	0.21	0.33
	DPCC+ASCDO	0.41	0.38	0.05	0.06
$R = 10R_0$	DPCC	0.15	0.1	0.18	0.401
	DPCC+SCDO	0.3	0.13	0.01	0.01
	DPCC+ASCDO	0.152	0.113	0.01	0.01
$L = 2L_0$	DPCC	1.42	0.63	0.35	0.22
	DPCC+SCDO	1.18	0.35	0.28	0.12
	DPCC+ASCDO	0.18	0.25	0.1	0.05
$\Psi = 4\,\Psi_{f0}$	DPCC	0.14	0.21	0.082	3.49
	DPCC+SCDO	0.16	0.22	0.08	0.05
	DPCC+ASCDO	0.1	0.12	0.01	0.02

control performance for three control methods, when different parameter mismatches, i.e., $R{=}\,0.1\mathrm{R}_0$, $L{=}\,0.5\mathrm{L}_0$, and $\psi_f = 0.25\,\psi_{f0}$, coexist in control system. And the quantitative comparison of three control methods is given by Table III can be obtained from the response. It is obvious that the steady-state errors exist in the *d*- and *q*-axis current responses of DPCC method under the parameter mismatch. Moreover, according to the quantitative comparison, it can be clearly shown that the influence of the steady-state errors can be effectively suppressed by using the proposed DPCC + SCDO and DPCC + ASCDO methods. The i_d steady-state error of DPCC + SCDO is maximally reduced by up to 59%, from 0.52 to 0.21 A. The i_q steady-state error of DPCC + SCDO is maximally reduced by up to 98%, from 3.49 to 0.05 A. On the anther hand, the i_d steady-state error of DPCC + ASCDO is maximally reduced by up to 90%, from 0.52 to 0.05 A. The i_q steady-state error of DPCC + ASCDO is maximally reduced by up to 99%, from 3.49 to 0.02 A. In addition, the quantitative comparison confirms that DPCC + ASCDO method has satisfying steady-state performance (ripples of i_d and i_q) compared with DPCC + SCDO method, since the sliding-mode chattering of ASCDO is reduced effectively by using the novel sliding-mode reaching law.

In order to further evaluate the performance of proposed method, the experiments are completed when a step change of parameter occurs during the operation. The experimental results are shown in Fig. 14. At 1.5 s, the parameters steps from R_0,

L_0, and ψ_{f0} to $1.5\mathrm{R}_0$, $0.5\mathrm{L}_0$, and 0.5 ψ_{f0}. From the results, it can be seen that proposed methods (DPCC + SCDO and DPCC + ASCDO) are able to suppress the disturbances caused by step change of parameters during the system operation.

In sum, simulation and experimental results verify the effectiveness of the proposed DPCC + SCDO and DPCC + ASCDO methods.

The proposed method can also be applied to IPMSM control system. However, it cannot be discussed here due to lack of space.

VII. Conclusion

In this paper, one novel DPCC method was proposed and experimentally applied to a PMSM system. The major contributions of this paper include the following:

1) in order to simultaneously predict future value of stator current and track parameter disturbances in real time, a SCDO is presented;
2) a composite control algorithm combining DPCC and SCDO (DPCC + SCDO) is developed to improve the control performance of PMSM system;
3) a novel sliding-mode exponential reaching law is introduced to suppress the sliding-mode chattering of SCDO. And, the DPCC + ASCDO method is developed to further improve the performance of DPCC + SCDO method.

References

[1] J. A. Suul, K. Ljøkelsøy, T. Midtsund, and T. Undeland, "Synchronous reference frame hysteresis current control for grid converter applications," *IEEE Trans. Ind. Electron.*, vol. 47, no. 5, pp. 2183–2194, Sep./Oct. 2011.

[2] M.P. Kazmierkowski and L. Malesani, "Current control techniques for three-phase voltage-source PWM converters: A survey," *IEEE Trans. Ind. Electron.*, vol. 45, no. 5, pp. 691–703, Oct. 1998.

[3] W. Xie, X. Wang, F. Wang, W. Xu, R. M. Kennel, and R. D. Lorenz, "Finite-control-set model predictive torque control with a deadbeat solution for PMSM drives," *IEEE Trans. Ind. Electron.*, vol. 62, no. 9, pp. 5402–5410, Sep. 2015.

[4] Y. Zhang and H. Yang, "Two-vector-based model predictive torque control without weighting factors for induction motor drives," *IEEE Trans. Power Electron.*, vol. 31, no. 2, pp. 1381–1390, Sep. 2016.

[5] Y. Zhang and H. Yang, "Model predictive torque control of induction motor drives with optimal duty cycle control," *IEEE Trans. Power Electron.*, vol. 29, no. 12, pp. 6593–6603, Dec. 2014.

[6] J. Guzinski and H. Abu-Rub, "Speed sensorless induction motor drive with predictive current controller," *IEEE Trans. Ind. Electron.*, vol. 60, no. 2, pp. 699–709, Jan. 2013.

[7] P. Cortes, M. P. Kazmierkowski, R. M. Kennel, D. E. Quevedo, and J. Rodriguez, "Predictive control in power electronics and drives," *IEEE Trans. Ind. Electron.*, vol. 55, no. 12, pp. 4312–4324, Dec. 2008.

[8] Y. Zhang and H. Yang, "Generalized two-vectors-based Model predictive torque control of induction motor drives," *IEEE Trans. Power Electron.*, vol. 30, no. 7, pp. 3818–3829, Jul. 2015.

[9] H. Liu and S. Li, "Speed control for PMSM servo system using predictive functional control and extended state observer," *IEEE Trans. Ind. Electron.*, vol. 59, no. 2, pp. 1171–1183, Feb. 2012.

[10] B.-J. Kang and C.-M. Liaw, "A robust hysteresis current-controlled PWM inverter for linear PMSM driven magnetic suspended positioning system," *IEEE Trans. Power Electron.*, vol. 48, no. 5, pp. 956–967, Oct. 2001.

[11] A. Dey, P. P. Rajeevan, R. Ramchand, K. Mathew, and K. Gopakumar, "A space-vector-based hysteresis current controller for a general n-level inverter-fed drive with nearly constant switching frequency control," *IEEE Trans. Ind. Electron.*, vol. 60, no. 5, pp. 1989–1998, May 2013.

[12] W. Song, J. Ma, L. Zhou, and X. Feng, "Deadbeat predictive power control of single-phase three-level neutral-point-clamped converters using space-vector modulation for electric railway traction," *IEEE Trans. Power Electron.*, vol. 31, no. 1, pp. 721–731, Jan. 2016.

[13] S. Li and Z. Liu, "Adaptive speed control for permanent magnet synchronous motor system with variations of load inertia," *IEEE Trans. Ind. Electron.*, vol. 56, no. 8, pp. 3050–3059, Aug. 2009.

[14] C.-K. Lin, T.-H. Liu, J.-T. Yu, L.-C. Fu, and C.-F. Hsiao, "Model-free predictive current control for interior permanent-magnet synchronous motor drives based on current difference detection technique," *IEEE Trans. Ind. Electron.*, vol. 61, no. 2, pp. 667–681, Feb. 2014.

[15] L. Springob and J. Holtz,"High-bandwidth current control for torque-ripple compensation in PM synchronous machines,"*IEEE Trans. Ind. Electron.*, vol. 45, no. 5, pp. 713–720, Oct. 1998.

[16] M. Prendl and E. Schaltz, "Sensorless model predictive direct current control using novel second-order PLL observer for PMSM drive systems," *IEEE Trans. Ind. Electron.*, vol. 58, no. 9, pp. 4087–4095, Sep. 2011.

[17] M. Preindl, E. Schaltz, and P. Thogersen, "Switching frequency reduction using model predictive direct current control for high-power voltage source inverters," *IEEE Trans. Ind. Electron.*, vol. 58, no. 7, pp. 2826–2835, Jun. 2011.

[18] H. Liu and S. Li,"Speed control for PMSM servo system using predictive functional control and extended state observer,"*IEEE Trans. Ind. Electron.*, vol. 59, no. 2, pp. 1171–1183, Feb. 2012.

[19] P. Cortes, J. Rodriguez, C. Silva, and A. Flores, "Delay compensation in model predictive current control of a three-phase inverter," *IEEE Trans. Ind. Electron.*, vol. 59, no. 2, pp. 1323–1325, Feb. 2012.

[20] J. Moreno, J. Huerta, R. Gil, and S. Gonzalez, "A robust predictive current control for three-phase grid-connected inverters," *IEEE Trans. Ind. Electron.*, vol. 56, no. 6, pp. 1993–2004, Jun. 2009.

[21] Y. Zhang, J. Zhu, and W. Xu, "Analysis of one step delay in direct torque control of permanent magnet synchronous motor and its remedies," in *Proc. Int Elect. Mach. Syst. Conf.*, 2010, pp.792–797.

[22] L. Tong *et al.*, "An SRF-PLL-based sensorless vector control using the predictive deadbeat algorithm for the direct-driven permanent magnet synchronous generator," *IEEE Trans. Power Electron.*, vol. 29, no. 6, pp. 2837–2849, Jun. 2014.

[23] P. Wipasuramonton, Z. Q. Zhu, and D. Howe, "Predictive current control with current-error correction for PM brushless AC drives," *IEEE Trans. Ind. Appl.*, vol. 42, no. 4, pp. 1071–1079, Jul. 2006.

[24] L. Niu, M. Yang, and D. Xu "An adaptive robust predictive current control for PMSM with online inductance identification," *Int. Rev. Elect. Eng.*, vol. 7, no. 2, pp. 3845–3856, 2012.

[25] H. Le-Huy, K. Slimani, and P. Viarouge, "Analysis and implementation of a real-time predictive current controller for permanent-magnet synchronous servo drives," *IEEE Trans. Ind. Electron.*, vol. 41, no. 1, pp. 110–117, Feb. 1994.

[26] W.-H. Chen, D. J. Ballance, P. J. Gawthrop, J. J. Gribble, and J. O'Reilly, "Nonlinear PID predictive controller," *Proc. Inst. Elect. Eng. Control Theory Appl.*, vol. 144, no. 6, pp. 603–611, Nov. 1999.

[27] W.-H. Chen, D. J. Ballance, P. J. Gawthrop, J. J. Gribble, and J. O'Reilly, "Design of a prediction-accuracy-enhanced continuous-time MPC for disturbed systems via a disturbance observer" *IEEE Trans. Ind. Electron.*, vol. 62, no. 9, pp. 5807–5816, Sep. 2015.

[28] J. Yang, S. Li, and X. Yu, "Sliding-mode control for systems with mismatched uncertainties via a disturbance observer," *IEEE Trans. Ind. Electron.*, vol. 60, no. 1, pp. 160–169, Jan. 2013.

[29] J. Yang and W. X. Zheng, "Offset-free nonlinear MPC for mismatched disturbance attenuation with application to a static var compensator," *IEEE Trans. Circuits Syst. II, Exp. Briefs*, vol. 61, no. 1, pp. 49–53, Jan. 2014.

[30] J. Yang, J. Su, S. Li, and X. Yu, "High-order mismatched disturbance compensation for motion control systems via a continuous dynamic sliding mode approach," *IEEE Trans. Ind. Inf.*, vol. 10, no. 1, pp. 604–614, Feb. 2014.

[31] Y. Shi, K. Sun, L. Huang, and Y. Li, "Online identification of permanent magnet flux based on extended Kalman filter for IPMSM drive with position sensorless control," *IEEE Trans. Ind. Electron.* vol. 59, no. 11, pp. 4169–4178, Nov. 2012.

[32] L. Springob and J. Holtz, "High-bandwidth current control for torque-ripple compensation in PM synchronous machines," *IEEE Trans. Ind. Electron.*, vol. 45, no. 5, pp. 713–721, Oct. 1998.

[33] W. Gao and J. C. Hung, "Variable structure control of nonlinear systems: A new approach," *IEEE Trans. Ind. Electron.*, vol. 40, no. 1, pp. 45–55, Feb. 1993.

[34] S. Kwak, S.-E. Kim, and J.-C. Park, "Predictive current control methods with reduced current errors and ripples for single-phase voltage source inverters," *IEEE Trans. Ind. Inf.*, vol. 11, no. 5, pp. 1006–1016, Oct. 2015.

Xiaoguang Zhang (M'15) was born in Heilongjiang, China, in 1985. He received the B.S. degree in electrical engineering from the Heilongjiang Institute of Technology, Harbin, China, in 2007, and the M.S. and Ph.D. degrees in electrical engineering from the Harbin Institute of Technology, Harbin, in 2009 and 2014, respectively.

He is currently an Assistant Professor at the North China University of Technology. From 2012 to 2013, he was a Research Associate at Wisconsin Electric Machines and Power Electronics Consortium (WEMPEC), University of Wisconsin–Madison, Madison. His current research interests include electric machines and drives.

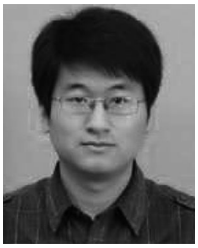

Benshuai Hou was born in Shandong, China, in 1989. He received the B.S. degree in electrical engineering from the Beijing Union University, Beijing, China, in 2013. He is currently working toward the M.S. degree at the North China University of Technology, Beijing.

His current research interests include PM machines and drives.

Yang Mei (M'15) received the B.S. degree from Xi'an Jiaotong University, Xian, China, in 2003, and the Ph.D. degree from Tsinghua University, Beijing, China, in 2008, both in electrical engineering.

In 2010, she was a Visiting Scholar with the Department of Energy Technology, Aalborg University, Denmark. She is currently an Associate Professor with the School of Electrical and Control Engineering, North China University of Technology, Beijing. Her current research interests include power electronics, ac motor drives, and renewable energy.